Conformal Miniaturization of Linear Arrays through a Two-Step Material-by-Design Approach

M. Salucci, G. Oliveri, N. Anselmi, and A. Massa

Abstract

In this work, a novel Material-by-Design (*MbD*) synthesis approach is proposed to address the conformal miniaturization of linear antenna arrays. The developed methodology exploits as a first step a quasi-conformal transformation optics (*QCTO*) algorithm to design a meta-material radome able to restore the desired radiation features of the radiating system once it has been made conformal to an arbitrary surface. Moreover, a second step based on a source inversion (*SI*) strategy is exploited in order to miniaturize the conformal architecture, by reducing the number of required radiators in the final conformal arrangement. Some numerical results are shown based on full-wave analyses in order to validate the effectiveness, as well as the current limitations, of the proposed design technique.

1 Spline Profile #2 - $N' = 20$

1.1 Validation vs. Lens Thickness (s)

- **Virtual & Physical Geometries**

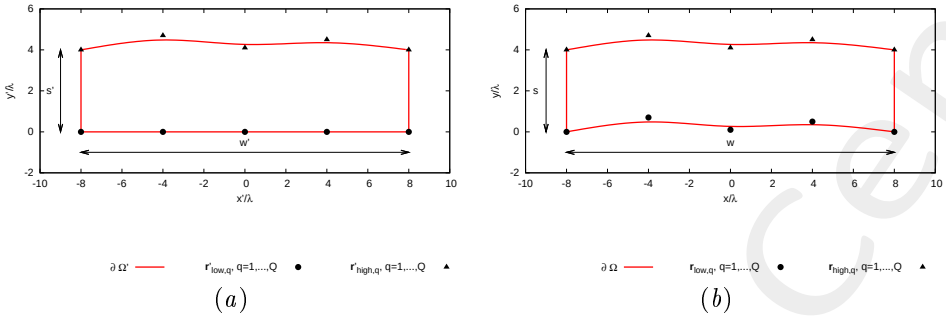

(a) (b)

Figure 1: Transformation regions and geometric parameters of interest.

- Width: $w = w' = 16.0$ $[\lambda]$;
- Lens thickness: $s = s' = \{4.0; 2.0\}$ $[\lambda]$;
- Number of spline control points: $Q = 5$;
- Control points in physical geometry:
  - $x_{low,q} \in [-w/2, w/2]$, $q = 1, ..., Q$ (equally-distributed);
  - $x_{high,q} = x_{low,q}$, $q = 1, ..., Q$;

$y_{low,1}$ $[\lambda]$	$y_{low,2}$ $[\lambda]$	$y_{low,3}$ $[\lambda]$	$y_{low,4}$ $[\lambda]$	$y_{low,5}$ $[\lambda]$
0.0	0.7	0.1	0.5	0.0

Table I: y-coordinate of the control points for the lower spline in physical space.

  - $y_{high,q} = (y_{low,q} + s)$, $q = 1, ..., Q$;
- Control points in virtual geometry:
  - $x'_{low,q} = x_{low,q}$, $q = 1, ..., Q$; $y'_{low,q} = 0.0$, $q = 1, ..., Q$;
  - $x'_{high,q} = x_{high,q}$, $q = 1, ..., Q$; $y'_{high,q} = y_{high,q}$, $q = 1, ..., Q$;

- **Virtual Array**
  - Number of elements, spacing, aperture: $N' = 20$, $d' = \frac{\lambda}{2}$, $L' = 9.5$ $[\lambda]$;
  - Distance from PEC ground plane (placed at $y' = 0.0$): $\delta' = \frac{\lambda}{4}$;
  - Excitations: $I_n = 1.0$, $\varphi_n = \frac{-2\pi}{\lambda} x_n sin(\phi_s + 90)$; $n = 1, ..., N'$;

- **QCTO**
  - Discretization cell dimension: 0.15 $[\lambda]$ (0.01 $[\lambda]$ for source mapping);

1.1.1 Results of the Transformation

Transformation Grids

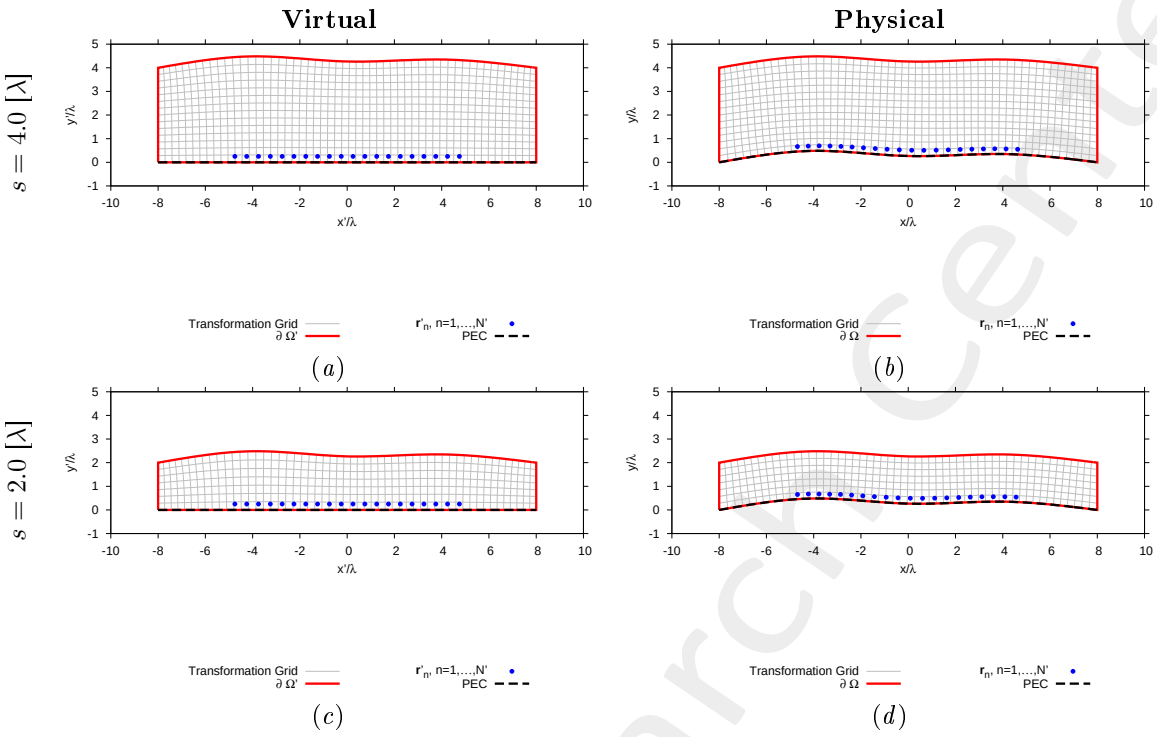

Figure 2: Transformation grids for virtual and physical geometries.

Lens Permittivity - $s = 4.0$ **[**λ**]**

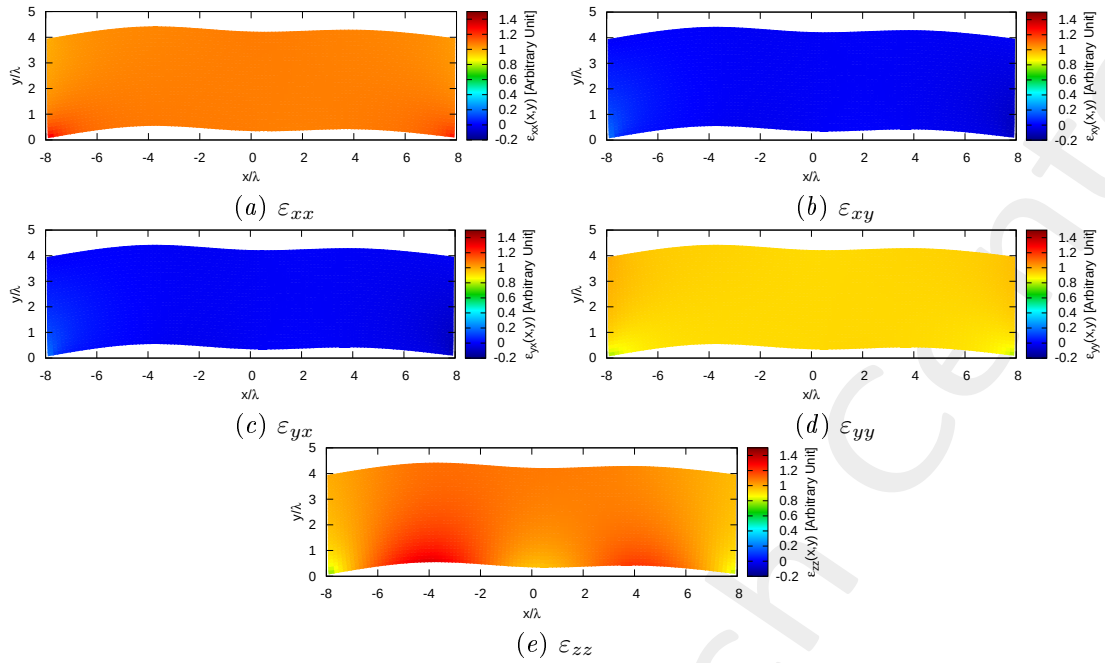

(a) ε_{xx} (b) ε_{xy} (c) ε_{yx} (d) ε_{yy} (e) ε_{zz}

Figure 3: Components of the relative permittivity tensor of the lens.

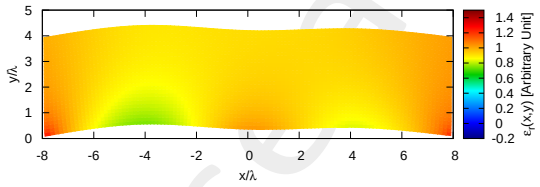

Figure 4: Isotropic approximate permittivity distribution of the lens.

Lens Permittivity - $s = 2.0$ **[**λ**]**

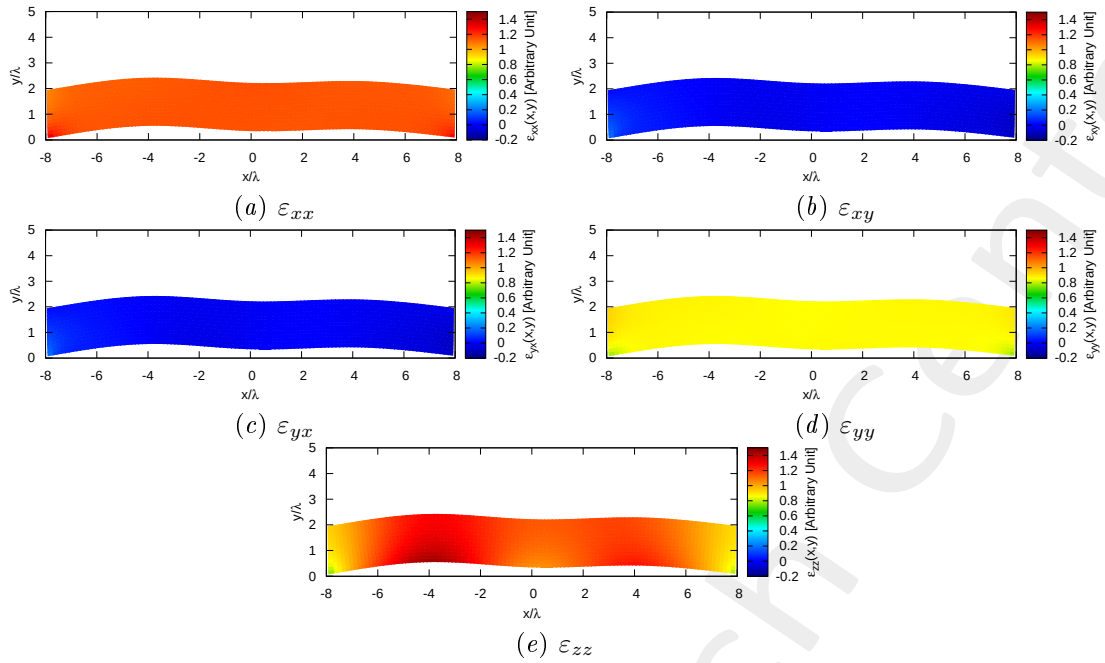

(a) ε_{xx} (b) ε_{xy} (c) ε_{yx} (d) ε_{yy} (e) ε_{zz}

Figure 5: Components of the relative permittivity tensor of the lens.

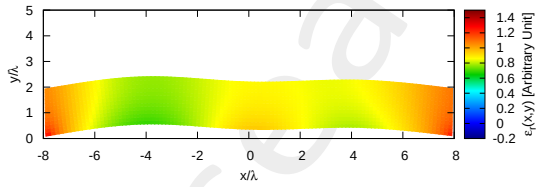

Figure 6: Isotropic approximate permittivity distribution of the lens.

Physical Lens Parameters

Lens Thickness $s = 4.0$ $[\lambda]$	
Anisotropic Permittivity Range	$[-0.11, 1.40]$
Isotropic Permittivity Range	$[0.00, 1.33]$
Lens Thickness $s = 2.0$ $[\lambda]$	
Anisotropic Permittivity Range	$[-0.11, 1.46]$
Isotropic Permittivity Range	$[0.00, 1.35]$

Table II: Permittivity ranges for the physical lens.

1.1.2 Far-Field Patterns (Aniso-Lens)

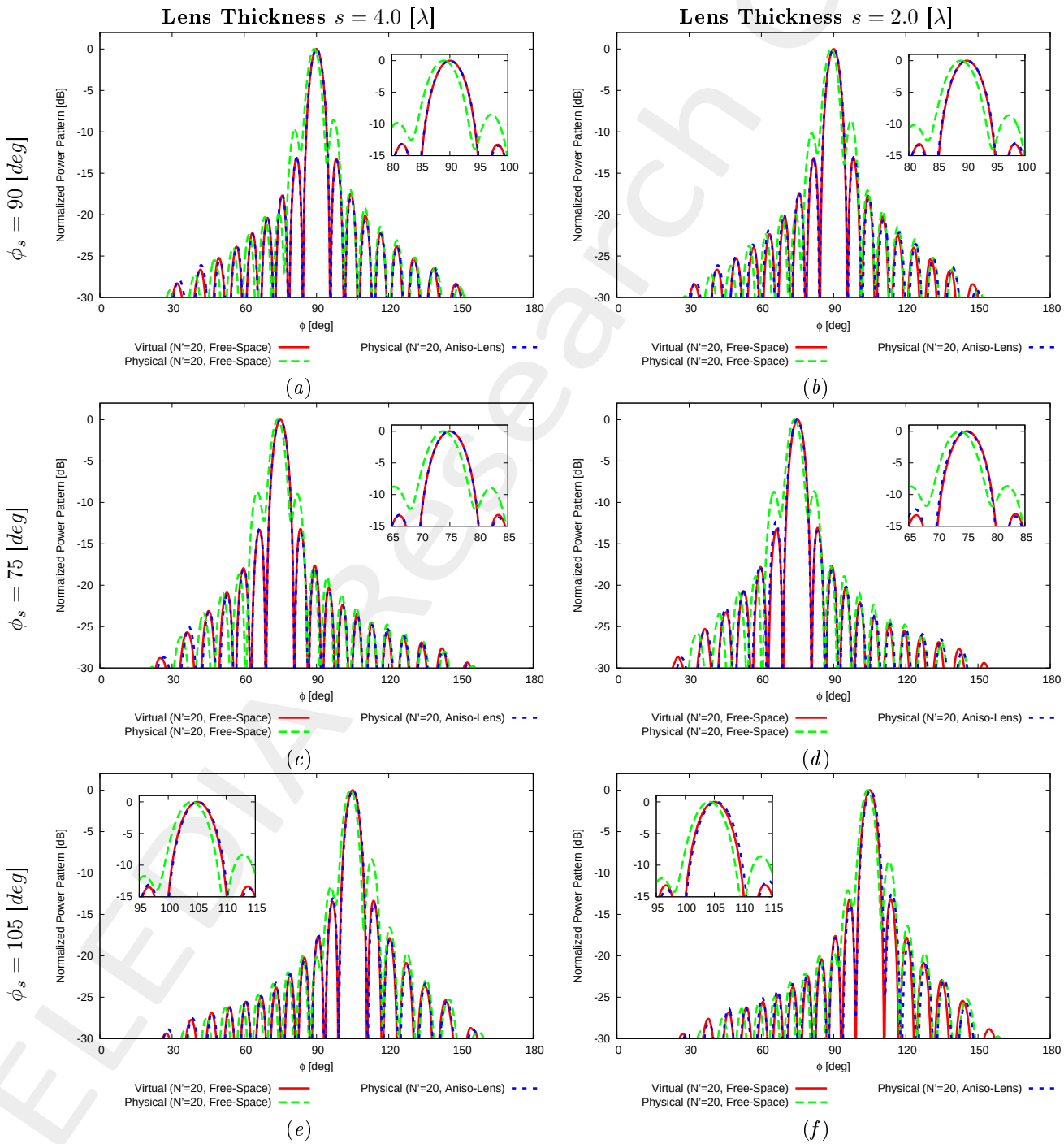

Figure 7: Comparison between the far field patterns.

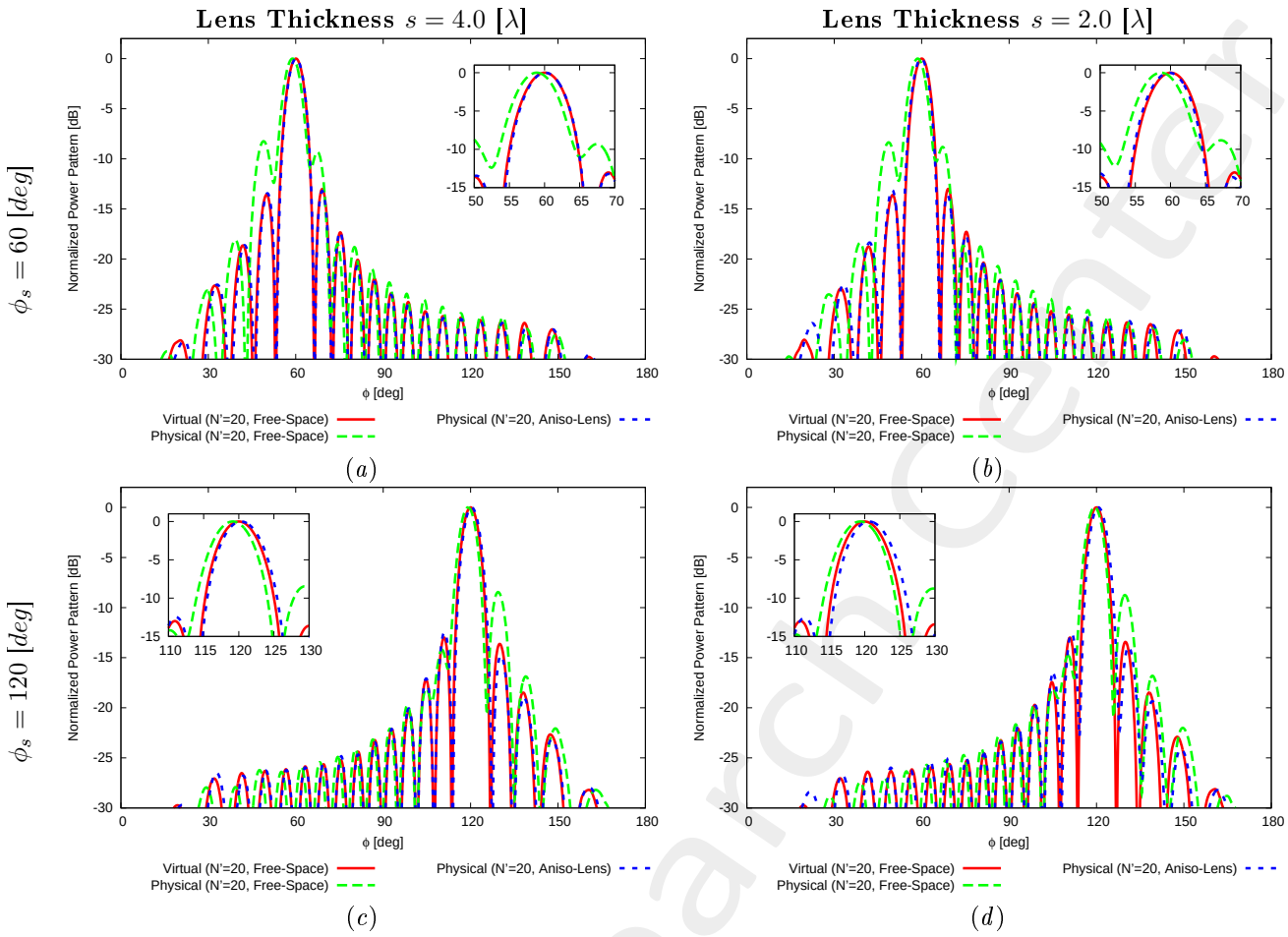

Figure 8: Comparison between the far field patterns.

1.2 Reduction of the Control Points through SI ($N' \rightarrow N < N'$)

Parameters

- Number of array elements before SI: $N' = 20$;
- Number of array elements after SI (N): check table below;
- Spacing after SI: $d = \lambda/2$;
- Radius of the observation domain: $r_{SI} = 50.0$ [λ];
- Number of field sampling points: $n_{SI} = 1000$.

	Before SI		**After SI**	
s [λ] (Lens Thickness)	N'	L [λ]	N	L [λ]
4.0	20	9.325	19	9.0
2.0	20	9.255	19	9.0

Table III: Parameters considered for SI.

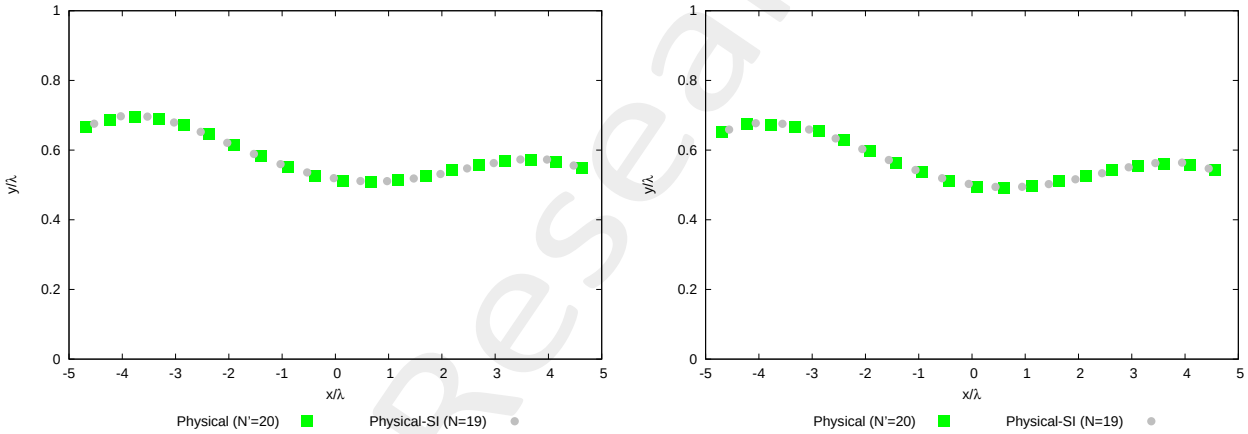

(a) $s = 4.0$ [λ] (b) $s = 2.0$ [λ]

Figure 9: Geometry of the physical array before (N') and after SI ($N < N'$).

Observations

- SI is not really necessary, since there is not a significant compression of the array.

1.2.1 Synthesized Excitations

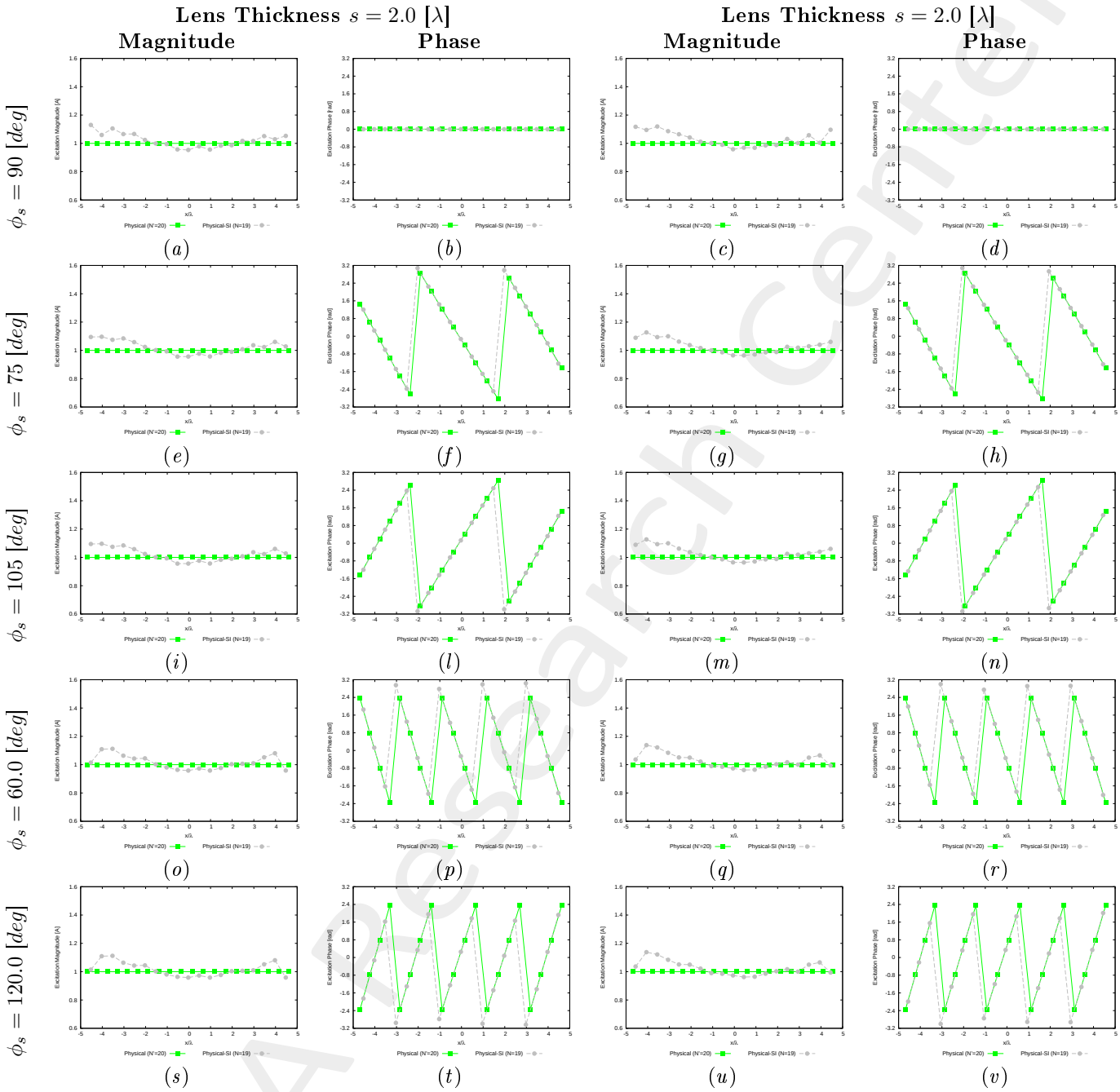

Figure 10: Magnitude and phase of the excitations of the physical array before (N') and after SI ($N < N'$).

1.2.2 Free-Space Far-Field Patterns (check SI)

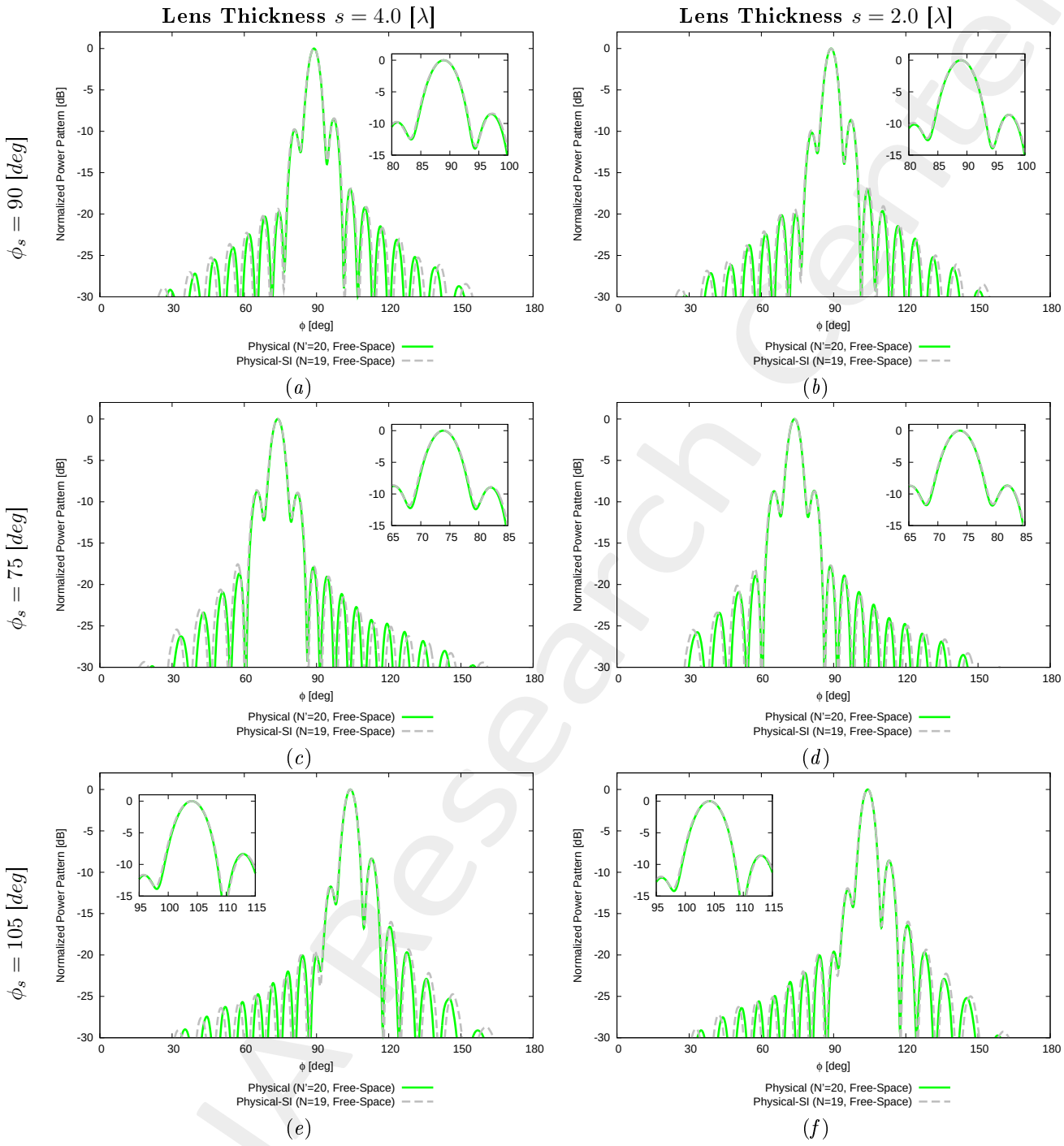

Figure 11: Free-Space patterns: Physical ($N' = 20$) vs. Physical-SI ($N < N'$).

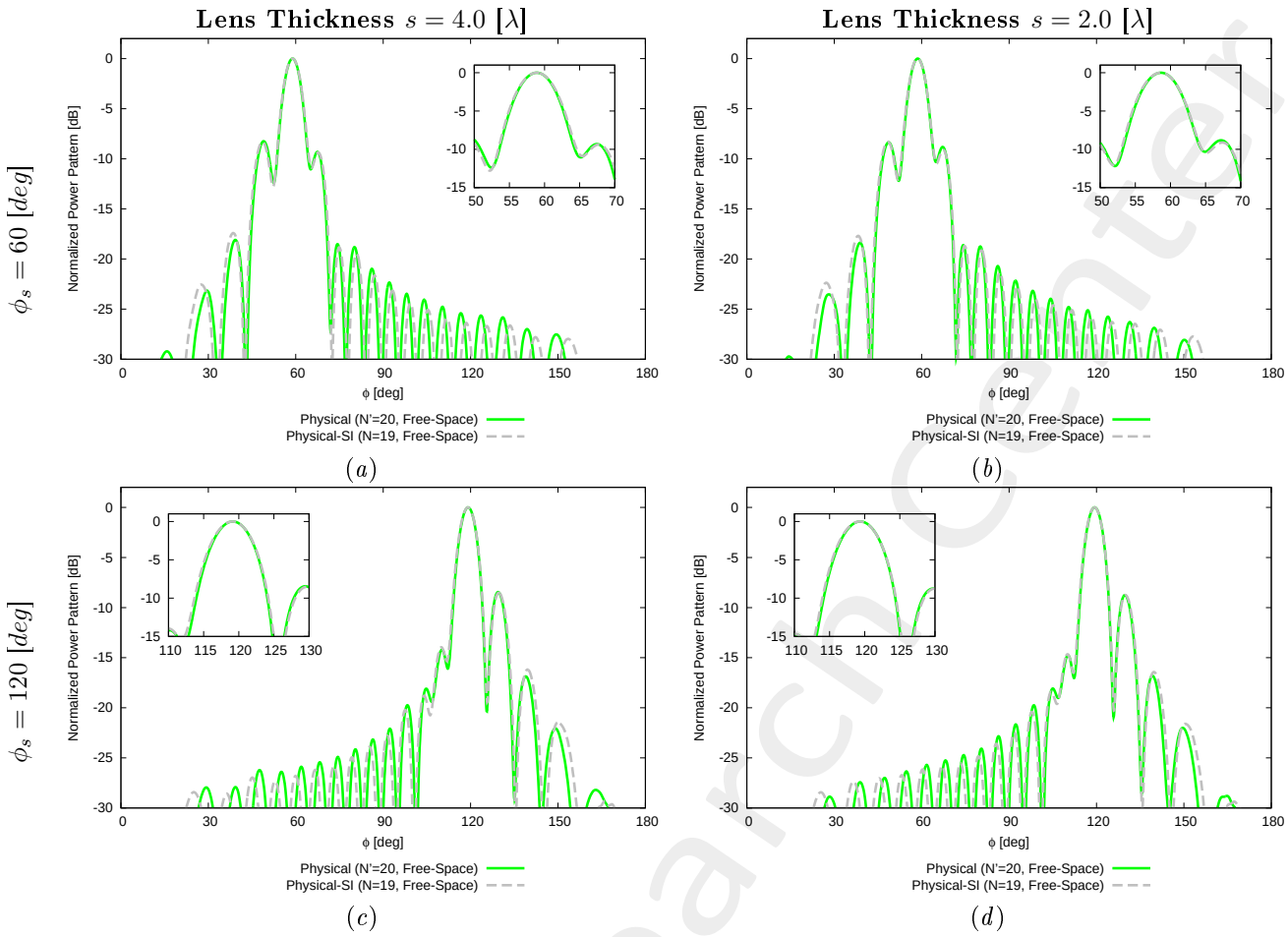

Figure 12: Comparison between the far field patterns.

1.2.3 Near-Field Distributions (Aniso-Lens, $\phi_s = 90$ [deg])

Lens Thickness $s = 4.0$ [λ]

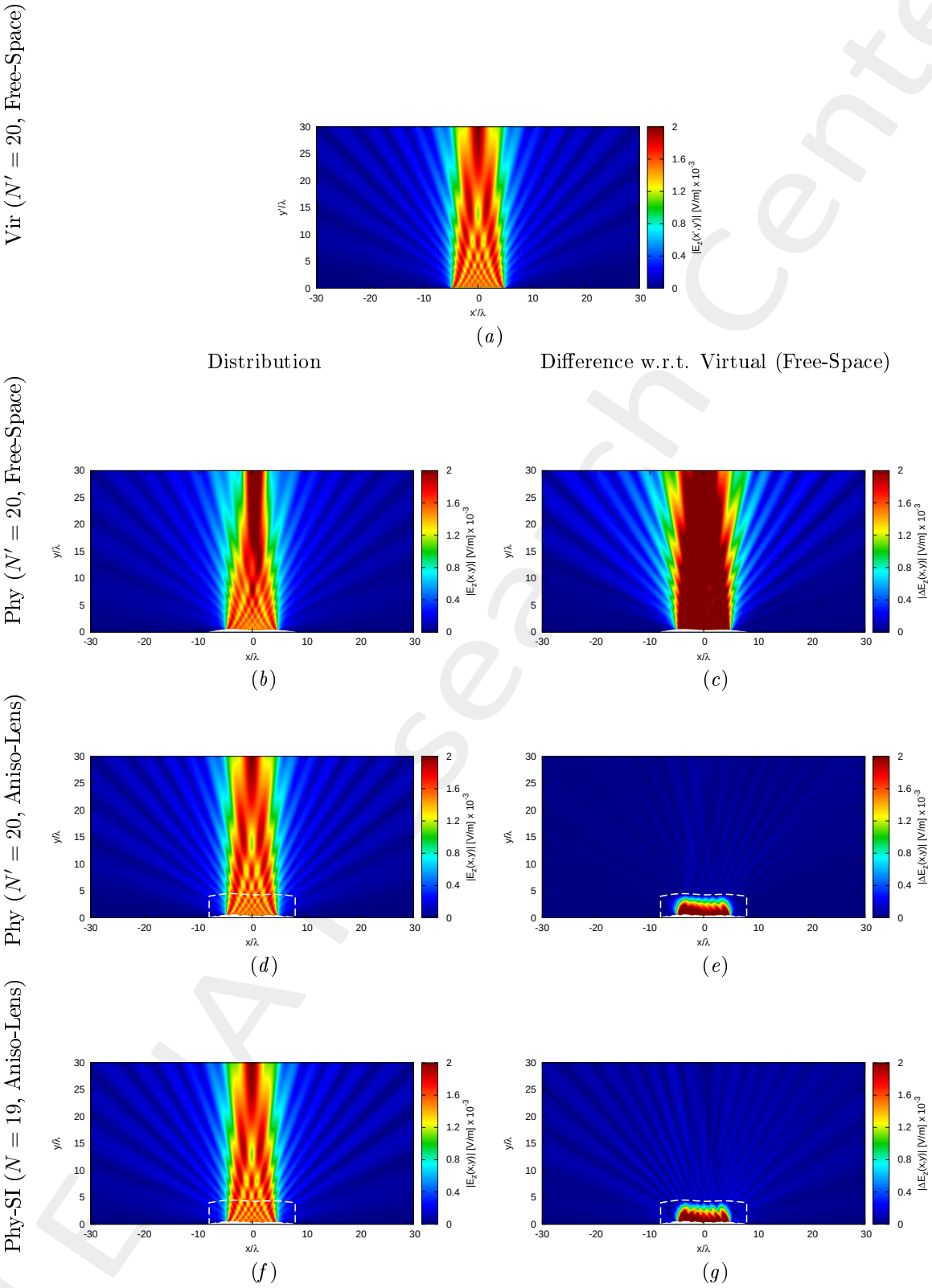

Figure 13: Lens Thickness $s = 4.0$ [λ] - Electric field distributions.

Lens Thickness $s = 2.0$ $[\lambda]$

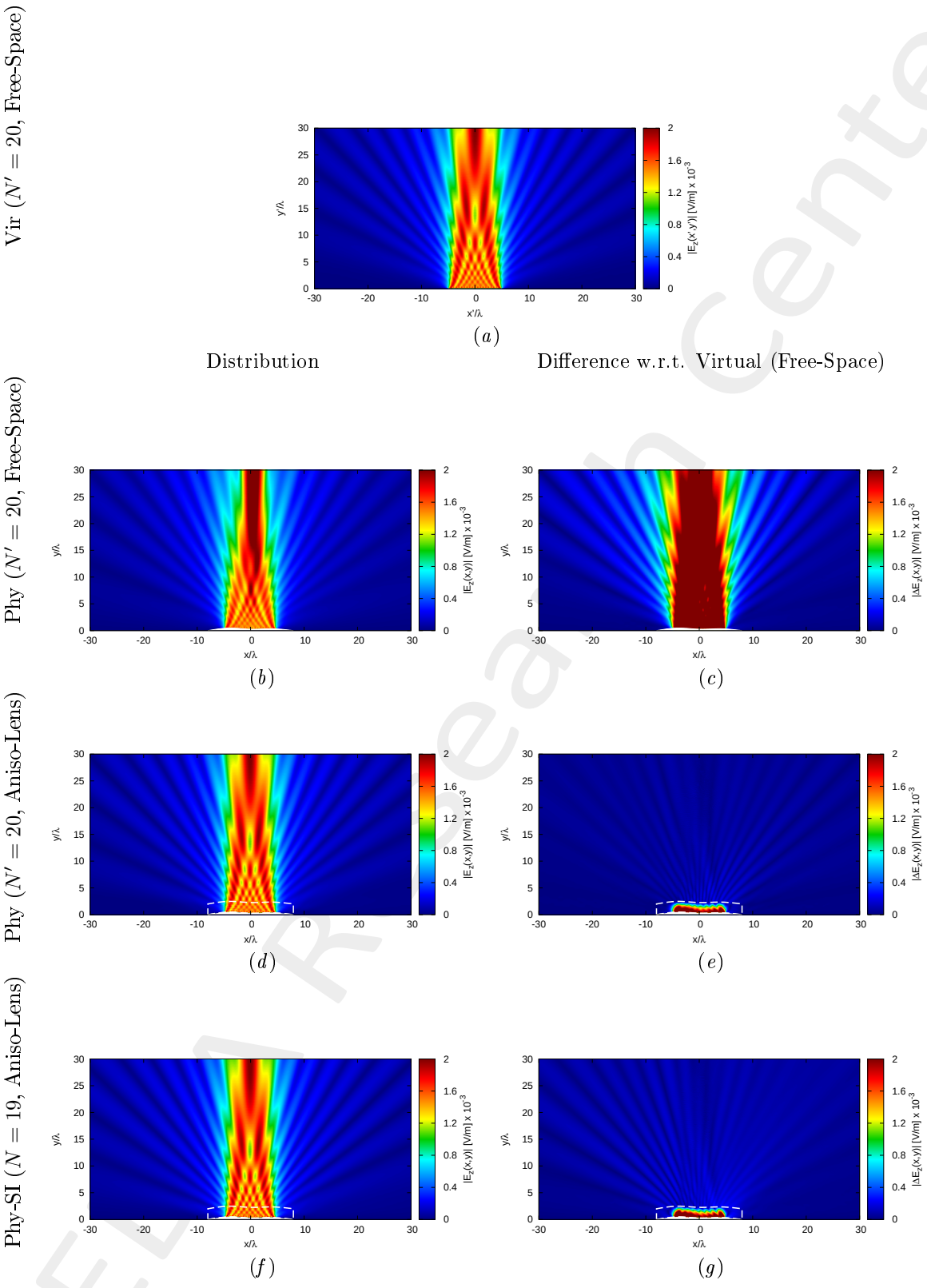

Figure 14: Lens Thickness $s = 2.0$ $[\lambda]$ - Electric field distributions.

1.2.4 Near-Field Distributions (Aniso-Lens, $\phi_s = 75$ [deg])

Lens Thickness $s = 4.0$ [λ]

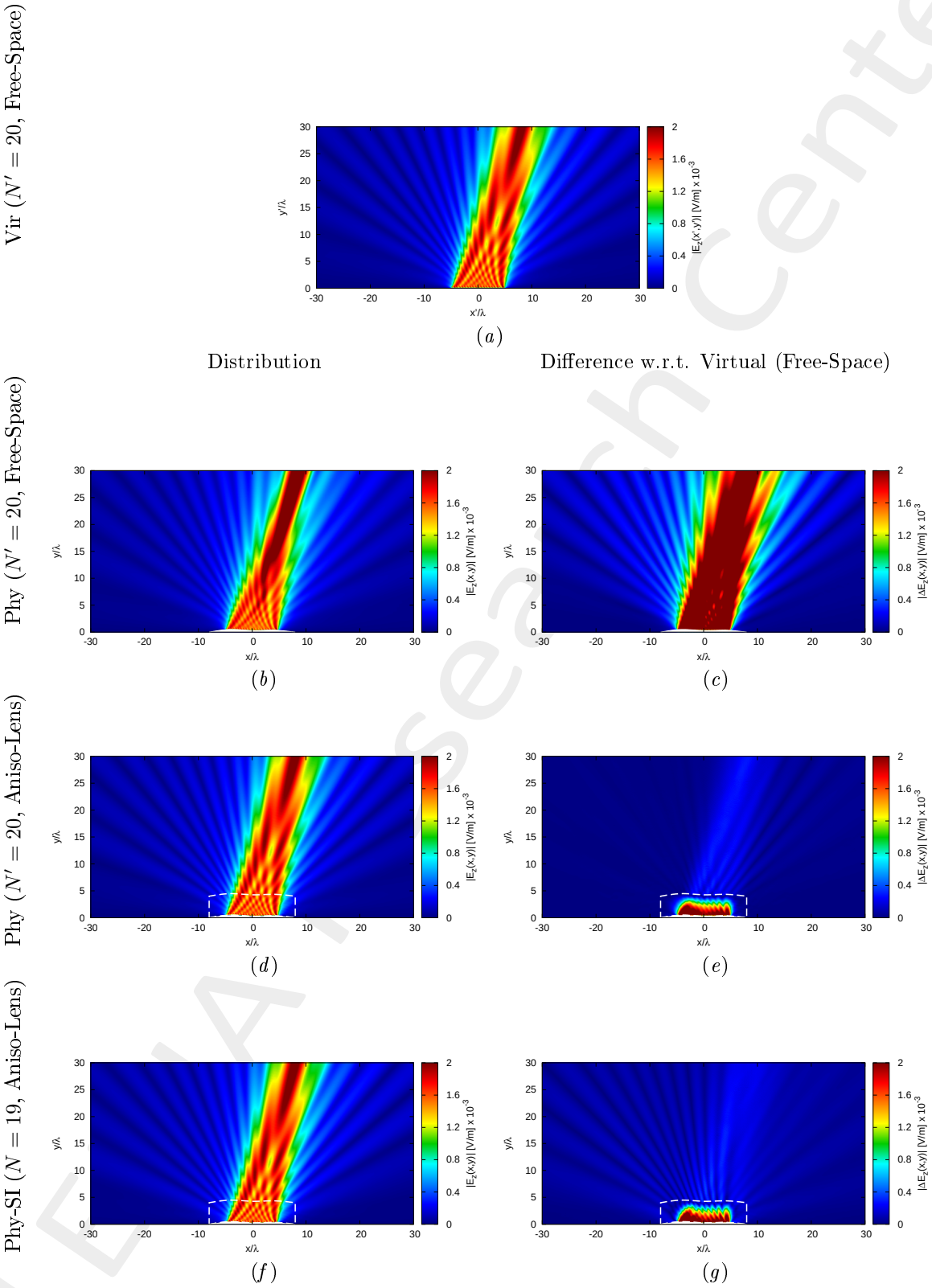

Figure 15: Lens Thickness $s = 4.0$ [λ] - Electric field distributions.

Lens Thickness $s = 2.0$ $[\lambda]$

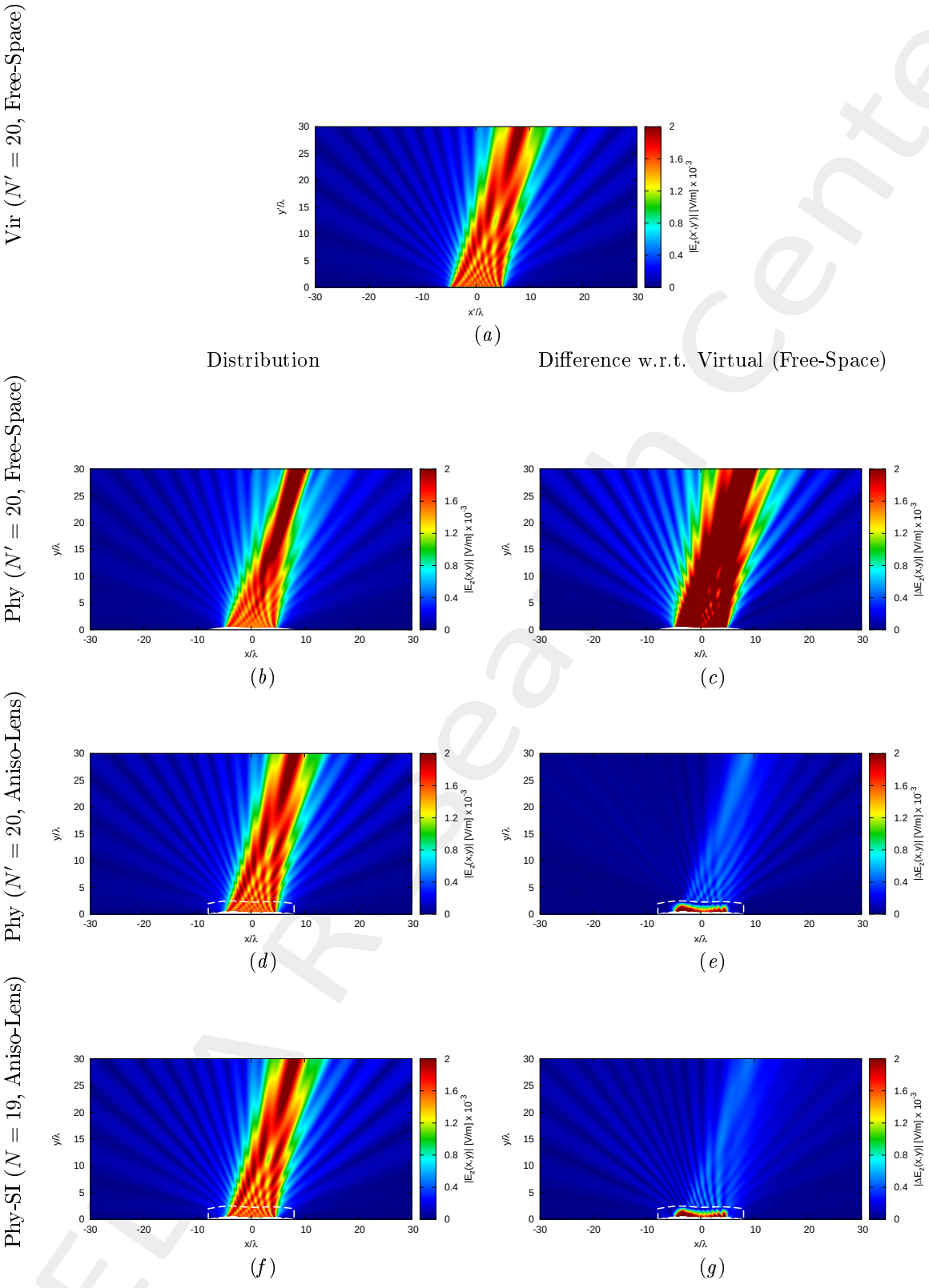

Figure 16: Lens Thickness $s = 2.0$ $[\lambda]$ - Electric field distributions.

1.2.5 Near-Field Distributions (Aniso-Lens, $\phi_s = 105$ [deg])

Lens Thickness $s = 4.0$ [λ]

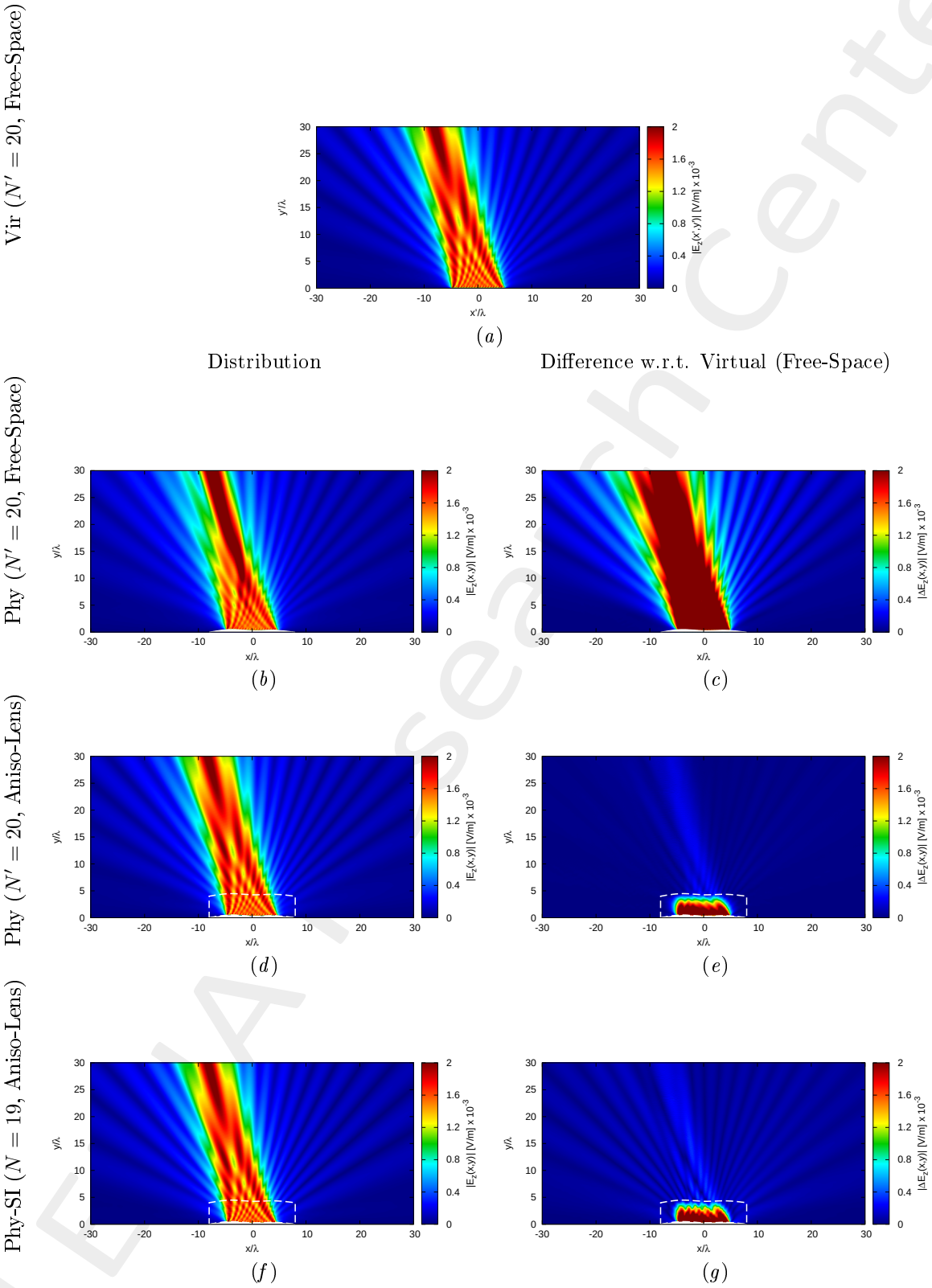

Figure 17: Lens Thickness $s = 4.0$ [λ] - Electric field distributions.

Lens Thickness $s = 2.0$ $[\lambda]$

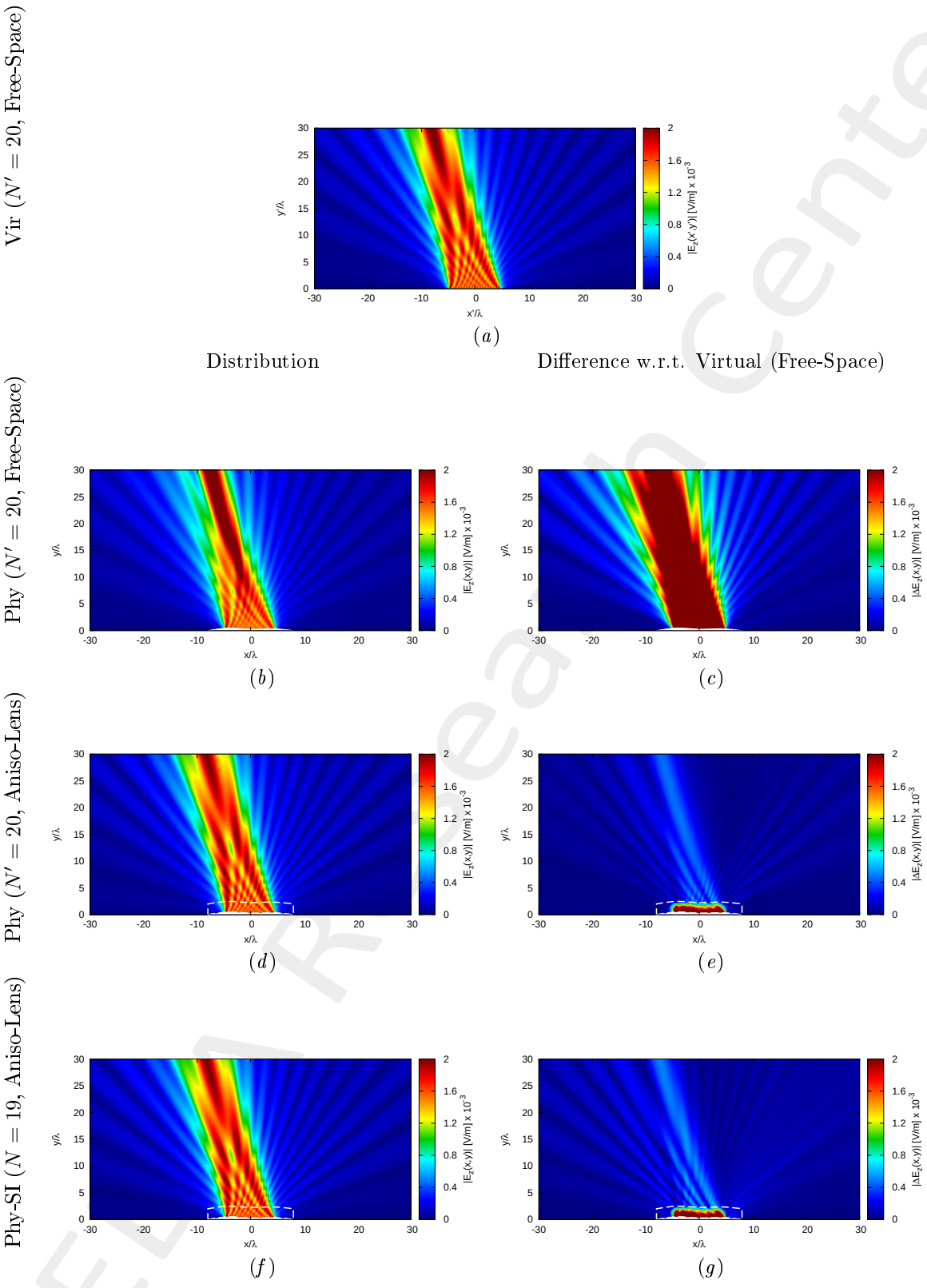

Figure 18: Lens Thickness $s = 2.0$ $[\lambda]$ - Electric field distributions.

1.2.6 Near-Field Distributions (Aniso-Lens, $\phi_s = 60$ [deg])

Lens Thickness $s = 4.0$ [λ]

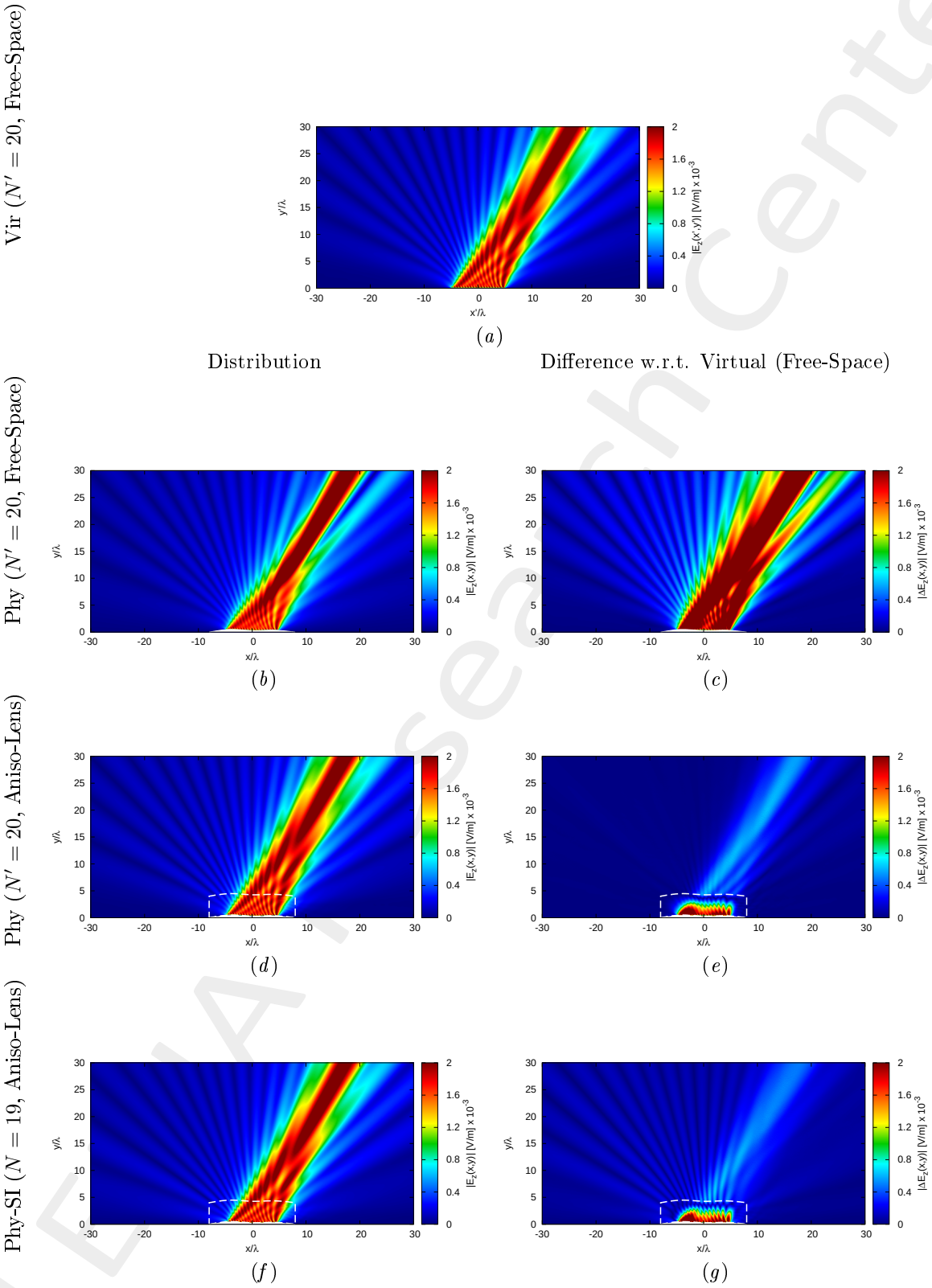

Figure 19: Lens Thickness $s = 4.0$ [λ] - Electric field distributions.

Lens Thickness $s = 2.0$ $[\lambda]$

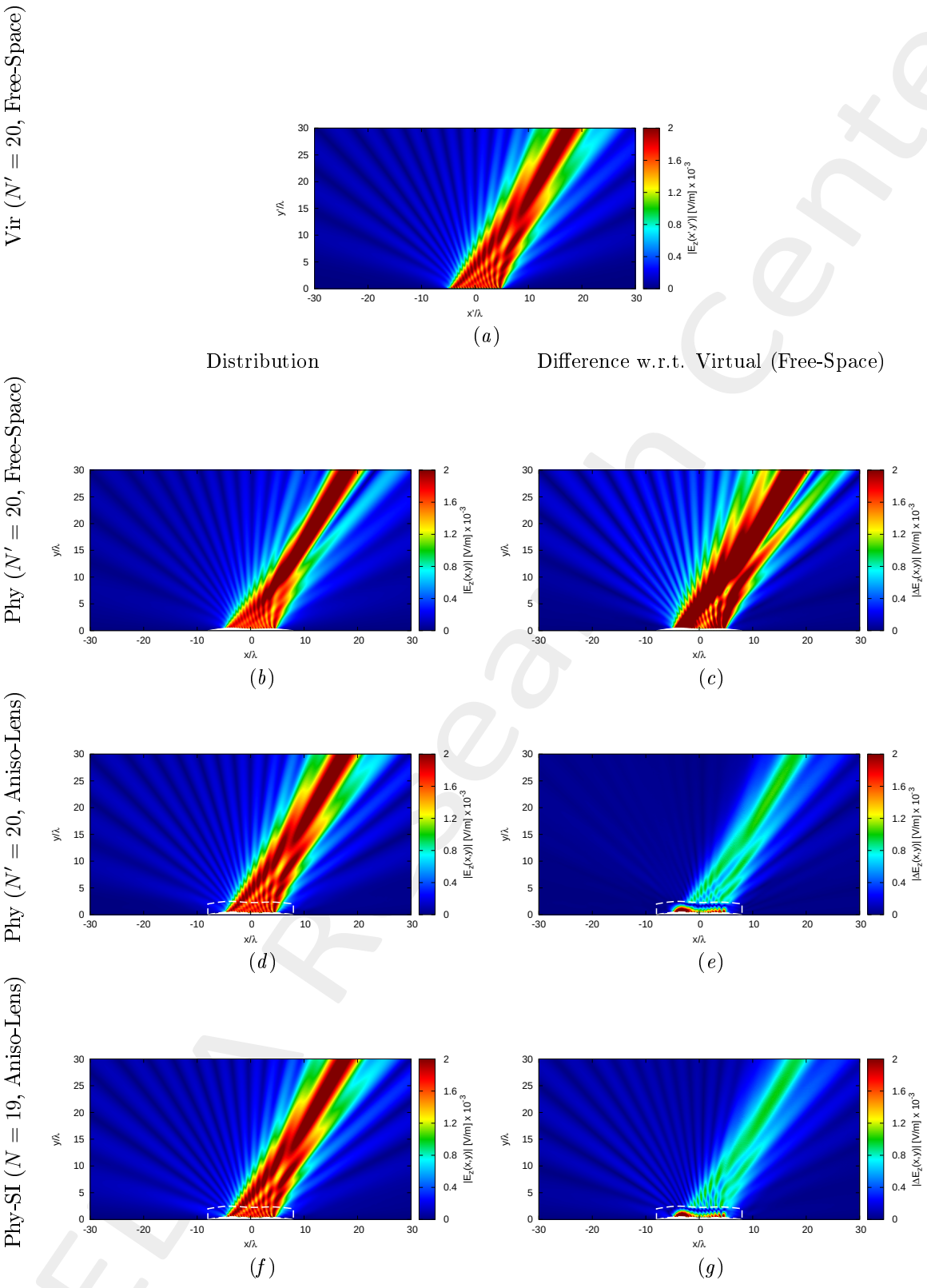

Figure 20: Lens Thickness $s = 2.0$ $[\lambda]$ - Electric field distributions.

1.2.7 Near-Field Distributions (Aniso-Lens, $\phi_s = 120$ [deg])

Lens Thickness $s = 4.0$ [λ]

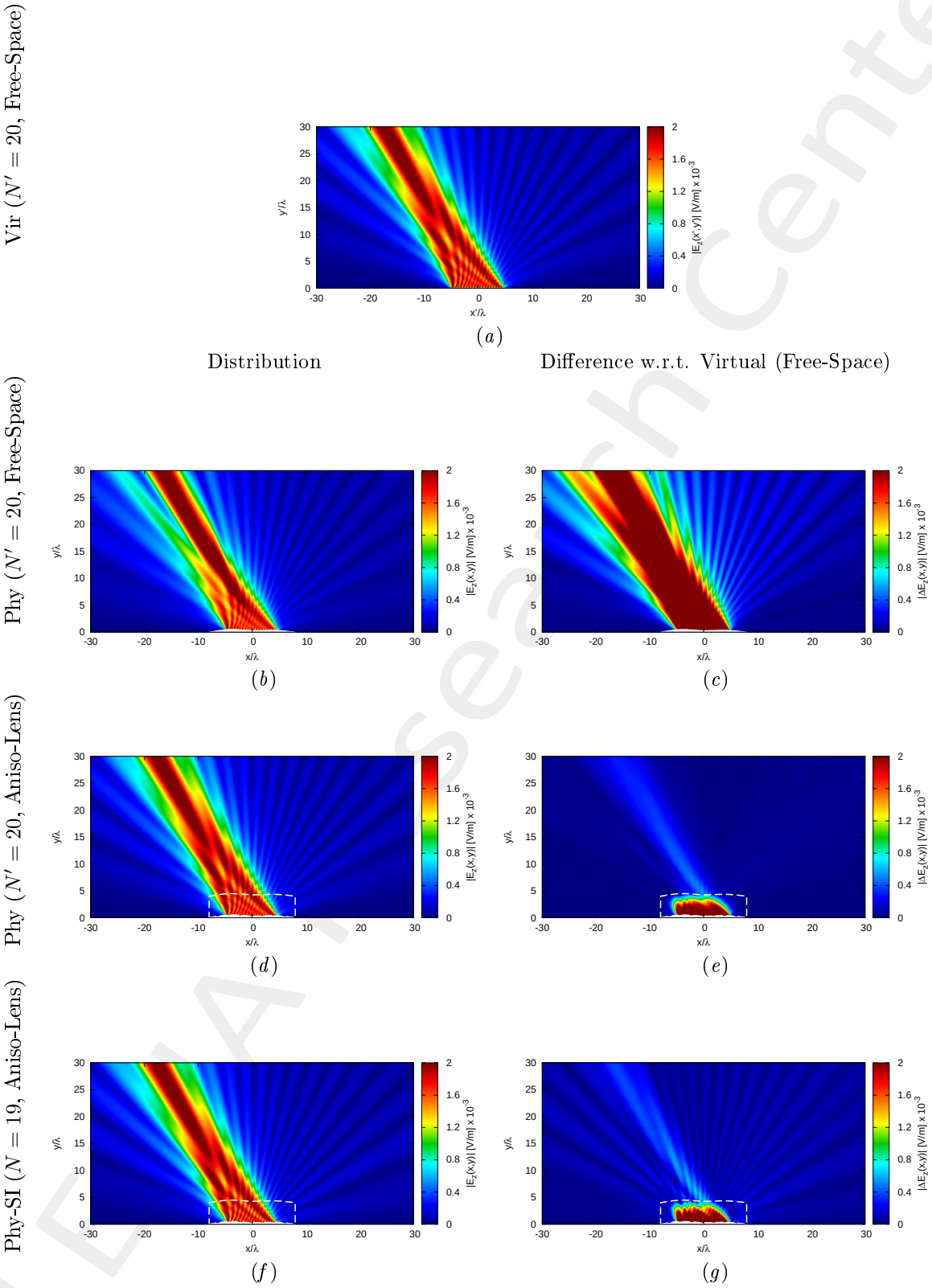

Figure 21: Lens Thickness $s = 4.0$ [λ] - Electric field distributions.

Lens Thickness $s = 2.0$ $[\lambda]$

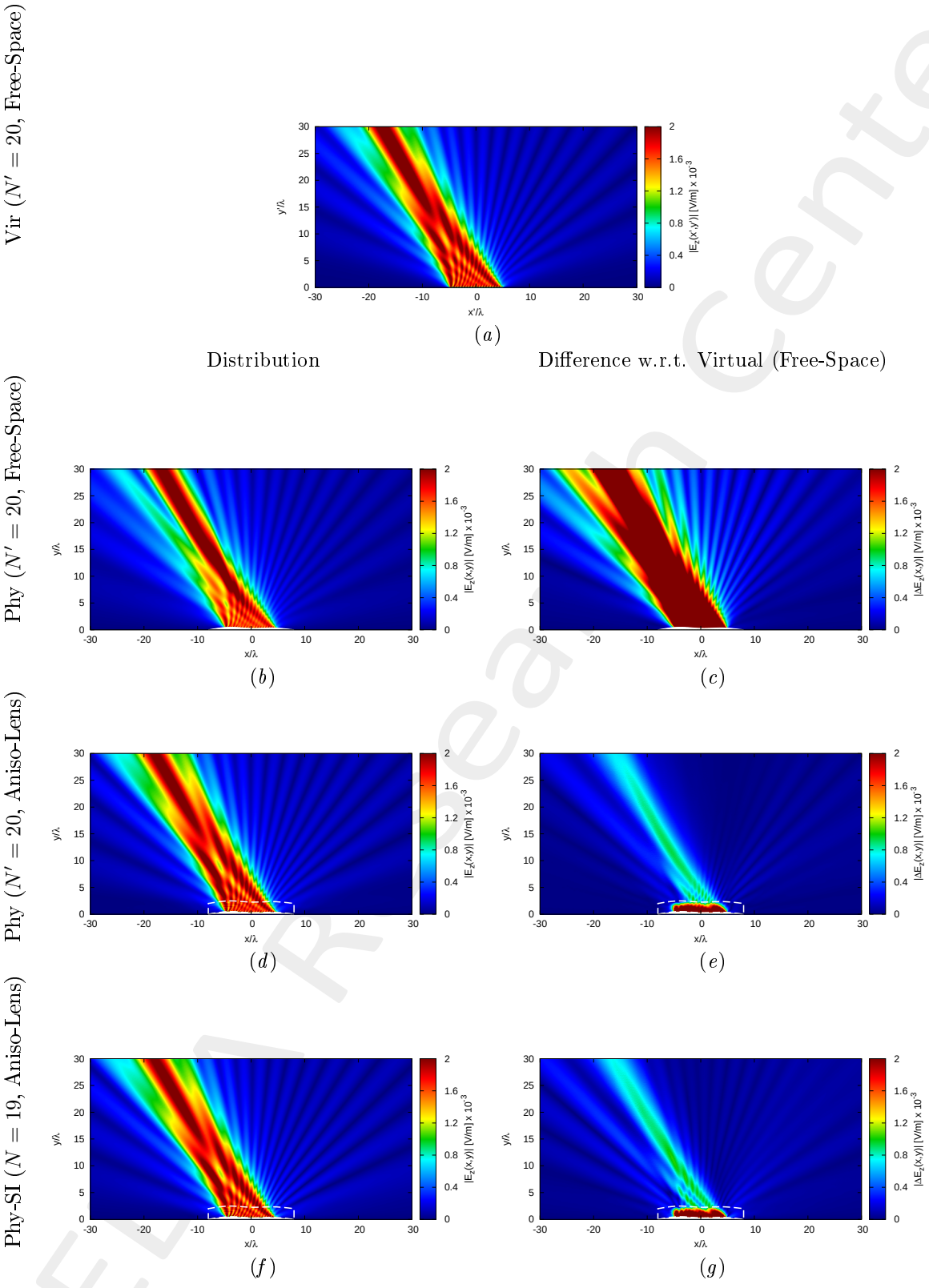

Figure 22: Lens Thickness $s = 2.0$ $[\lambda]$ - Electric field distributions.

1.2.8 Far-Field Patterns (Aniso-Lens)

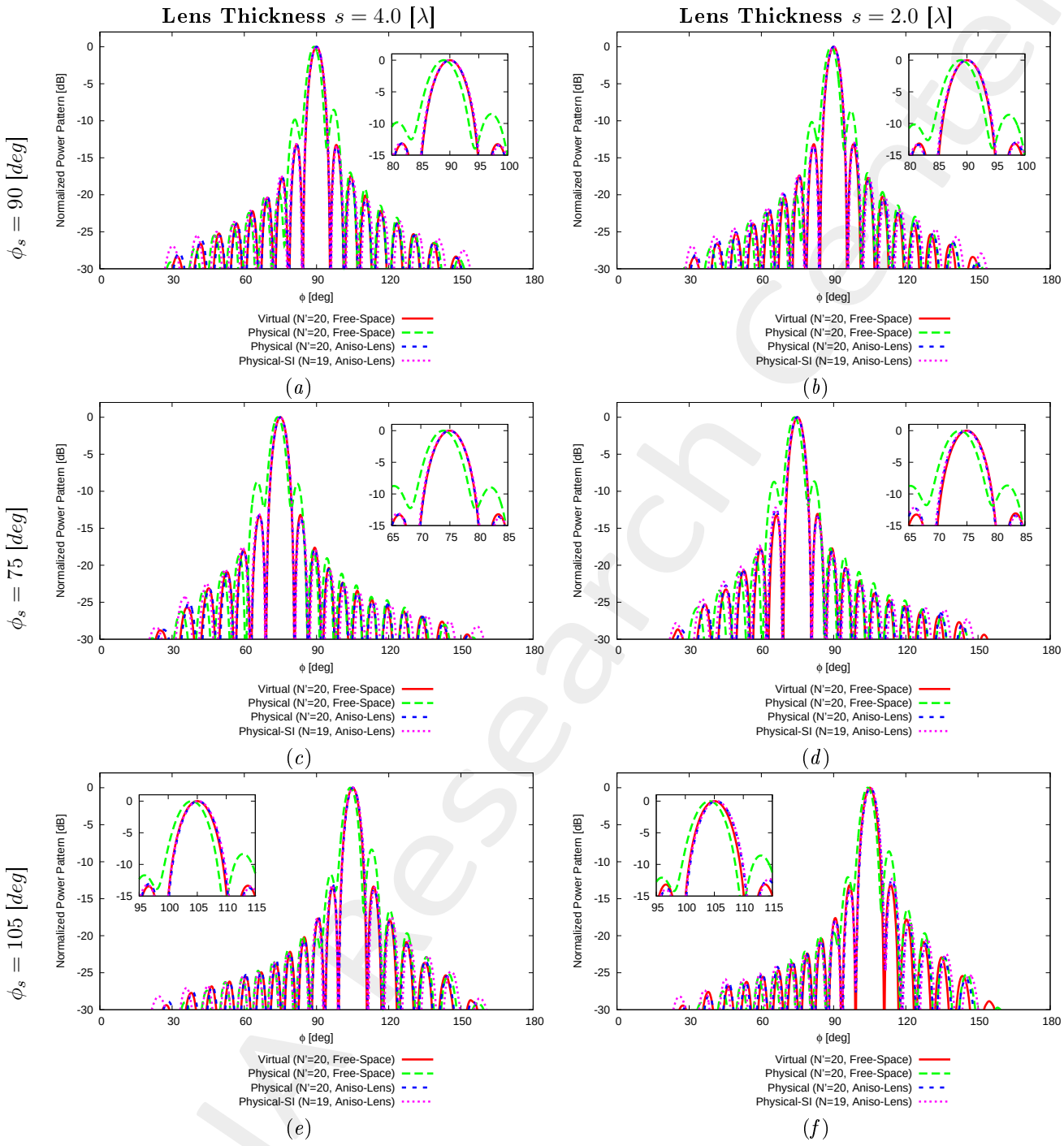

Figure 23: Comparison between the far field patterns.

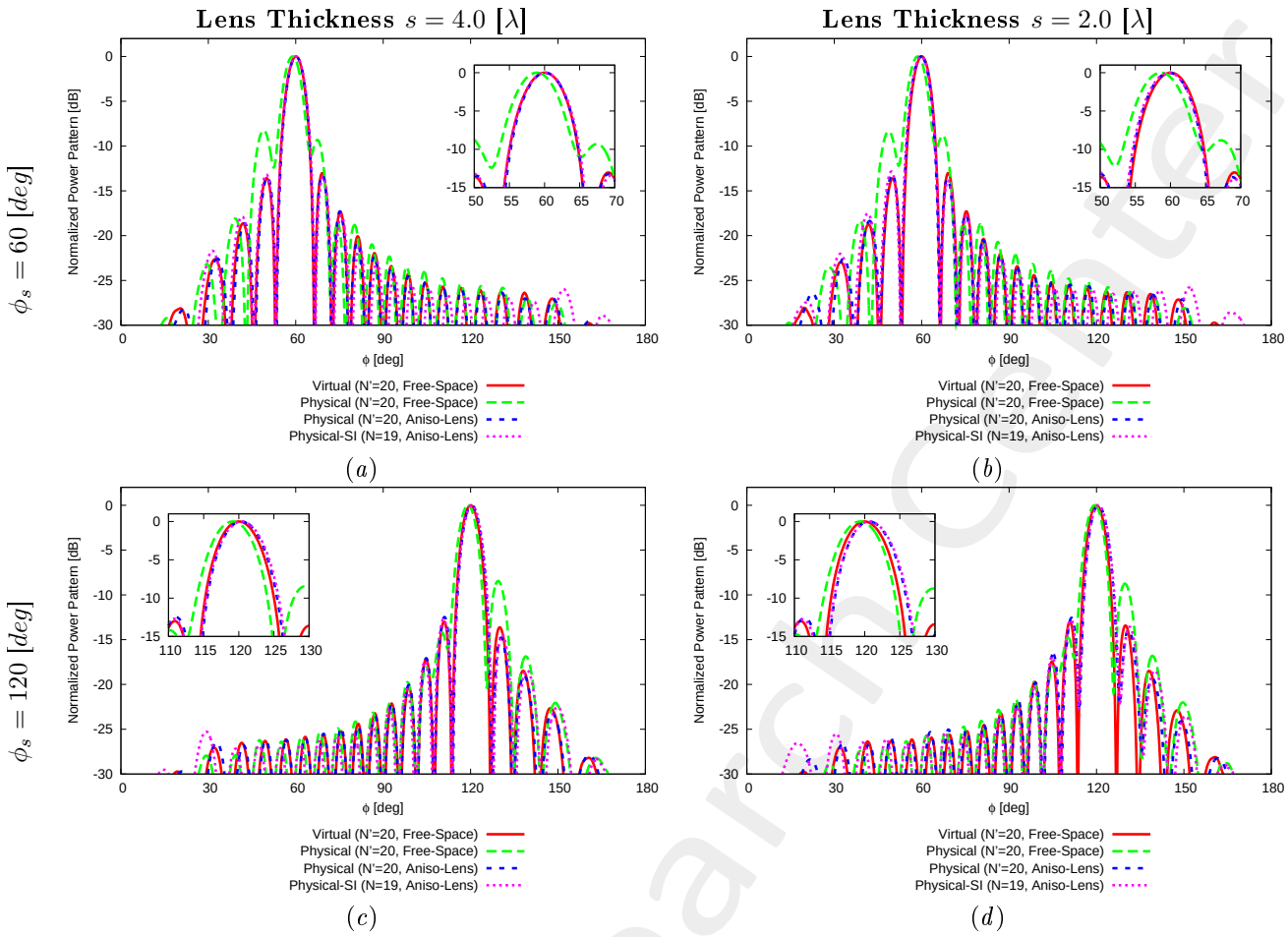

Figure 24: Comparison between the far field patterns.

References

[1] G. Oliveri, G. Gottardi, F. Robol, A. Polo, L. Poli, M. Salucci, M. Chuan, C. Massagrande, P. Vinetti, M. Mattivi, R. Lombardi, and A. Massa, "Co-design of unconventional array architectures and antenna elements for 5G base station," *IEEE Trans. Antennas Propag.*, vol. 65, no. 12, pp. 6752-6767, Dec. 2017.

[2] P. Rocca, G. Oliveri, R. J. Mailloux, and A. Massa, "Unconventional phased array architectures and design methodologies - A review," *Proc. IEEE*, vol. 104, no. 3, pp. 544-560, Mar. 2016.

[3] G. Oliveri, M. Salucci, N. Anselmi and A. Massa, "Multiscale System-by-Design synthesis of printed WAIMs for waveguide array enhancement," *IEEE J. Multiscale Multiphysics Computat. Techn.*, vol. 2, pp. 84-96, 2017.

[4] A. Massa and G. Oliveri, "Metamaterial-by-Design: Theory, methods, and applications to communications and sensing - Editorial," *EPJ Applied Metamaterials*, vol. 3, no. E1, pp. 1-3, 2016.

[5] L. Poli, G. Oliveri, P. Rocca, M. Salucci, and A. Massa, "Long-Distance WPT Unconventional Arrays Synthesis," *J. Electromagnet. Waves Appl.*, vol. 31, no. 14, pp. 1399-1420, Jul. 2017.

[6] G. Oliveri, F. Viani, N. Anselmi, and A. Massa, "Synthesis of multi-layer WAIM coatings for planar phased arrays within the system-by-design framework," *IEEE Trans. Antennas Propag.*, vol. 63, no. 6, pp. 2482-2496, Jun. 2015.

[7] G. Oliveri, L. Tenuti, E. Bekele, M. Carlin, and A. Massa, "An SbD-QCTO approach to the synthesis of isotropic metamaterial lenses," *IEEE Antennas Wireless Propag. Lett.*, vol. 13, pp. 1783-1786, 2014.

[8] G. Oliveri, D. H. Werner, and A. Massa, "Reconfigurable electromagnetics through metamaterials - A review" *Proc. IEEE*, vol. 103, no. 7, pp. 1034-1056, Jul. 2015.

[9] G. Oliveri, E. T. Bekele, M. Salucci, and A. Massa, "Transformation electromagnetics miniaturization of sectoral and conical horn antennas," *IEEE Trans. Antennas Propag.*, vol. 64, no. 4, pp. 1508-1513, Apr. 2016.

[10] G. Oliveri, E. T. Bekele, M. Salucci, and A. Massa, "Array miniaturization through QCTO-SI metamaterial radomes," *IEEE Trans. Antennas Propag.*, vol. 63, no. 8, pp. 3465-3476, Aug. 2015.

[11] G. Oliveri, E. T. Bekele, D. H. Werner, J. P. Turpin, and A. Massa, "Generalized QCTO for metamaterial-lens-coated conformal arrays," *IEEE Trans. Antennas Propag.*, vol. 62, no. 8, pp 4089-4095, Aug. 2014.

[12] G. Oliveri, E. Bekele, M. Carlin, L. Tenuti, J. Turpin, D. H. Werner, and A. Massa, "Extended QCTO for innovative antenna system designs," IEEE Antenna Conference on Antenna Measurements and Applications (CAMA 2014), pp. 1-3, Nov. 16-19, 2014.

[13] G. Oliveri, P. Rocca, M. Salucci, E. T. Bekele, D. H. Werner, and A. Massa, "Design and synthesis of innovative metamaterial-enhanced arrays," IEEE International Symposium on Antennas Propag. (APS/URSI 2013), Orlando, Florida, USA, pp. 972 - 973, Jul. 7-12, 2013.

[14] G. Oliveri, "Improving the reliability of frequency domain simulators in the presence of homogeneous metamaterials - A preliminary numerical assessment," *Progress In Electromagnetics Research*, vol. 122, pp. 497-518, 2012.

[15] M. Salucci, G. Oliveri, N. Anselmi, G. Gottardi, and A. Massa, "Performance enhancement of linear active electronically-scanned arrays by means of MbD-synthesized metalenses," *J. Electromagnet. Waves Appl.*, vol. 32, no. 8, pp. 927-955, 2018.

[16] M. Salucci, G. Oliveri, N. Anselmi, and A. Massa, "Material-by-design synthesis of conformal miniaturized linear phased arrays," *IEEE Access* (doi: 10.1109/ACCESS.2018.2833199).